

Negative-*U* Properties of the Deep Level E3 in ZnO

Rainer Pickenhain, Matthias Schmidt, Holger von Wenckstern,* Gabriele Benndorf, Andreas Pöpl, Rolf Böttcher, and Marius Grundmann

The deep level E3 is a commonly observed defect in bulk crystals and thin films of ZnO independently of the method of growth. Its chemical origin is still not finally understood. In this paper, previous research on the E3 level is reviewed and recent experimental results acquired by optical deep level transient spectroscopic (DLTS) methods are presented for the temperature range from 4 to 350 K, for photon energies between 0.25 and 4 eV, and for emission rates ranging from 10^{-3} to 10^4 s $^{-1}$. The capture cross section of the optical transition of E3-trapped electrons into the conduction band is described. Additionally, a second optical transition occurs for photon energies higher than 1 eV, which accounts for the lowering of the E3 DLTS signal at low temperatures under illumination. Further, it is unambiguously shown that the E3 defect can bind up to two electrons and that it has the properties of a negative-*U* center. Photoluminescence measurements reveal that the E3 defect is directly connected to a radiative recombination channel at 2.09 eV. Further, electron paramagnetic resonance (EPR) measurements were performed with optical excitation in dependence on the temperature and photon energy. Interestingly, the temperature-dependent EPR signal of V_O^+ is similar to that of the photo-ionization cross-section of the E3 defect. These experimental findings are discussed in comparison with published EPR results and results obtained by first-principle calculations of native point defects in ZnO.

1. Introduction

The wide band gap semiconductor ZnO has been investigated in detail for the last two decades. That research was motivated by the extraordinary material properties of ZnO, such as very high exciton binding energy, radiation hardness, a high fundamental band gap of about 3.4 eV, and consequent applications such as light emitting diodes, visible-blind photo-detectors, power


electronics and transparent electronic circuitry.^[1–3] However, ZnO is in general unipolar n-type^[4]; stable, high-quality p-type ZnO is still out of reach.^[5,6] On the other hand, high-quality n-type bulk crystals are available and serve as excellent substrates for homoepitaxial ZnO thin films. The free electron concentration in ZnO can be well controlled by doping with group III elements.^[7] Self-compensation by the spontaneous formation of intrinsic defects is, similarly to other wide band-gap semiconductors, an important mechanism limiting both n- and p-type dopability^[8] by the formation of zinc or oxygen vacancies, respectively.^[9–11] Experimentally, these intrinsic compensating defects have been studied by electron paramagnetic resonance (EPR), optically detected magnetic resonance (ODMR), and positron annihilation spectroscopy (PAS).^[12–15] Nevertheless, information about the electrical properties of such defects is scarce and/or controversial. Further, a direct electrical characterization of defects by temperature-dependent investigations such as deep-level transient spectroscopy (DLTS) has been limited to states with binding energies below 1 eV,^[16] which is only one-third

of ZnO's band gap. In order to investigate deeper states additional optical excitation is necessary for the determination of their photo-ionization cross-section.^[17–19] For the evaluation of the capacitance transients after an optical excitation, Chantre et al.^[18] use the initial slope of the transient whereas Brehme et al.^[17] search for the maximum of the signal within a rate window similar to a standard DLTS. The two methods are referred to as deep-level optical spectroscopy (DLOS), respectively, optical deep-level transient spectroscopy (ODLTS). Both methods are capable of quantifying the optical emission rates for electrons e_n^0 and holes e_p^0 ; the latter requires the use of a pn-junction in the case of a n-type semiconductor like ZnO. ODLTS measurements can be acquired at constant temperature (referred to as ODLTS($h\nu, T = \text{const}$)) or at a constant photon energy (referred to as ODLTS($h\nu = \text{const}, T$)).

In the present paper we have studied the virtually omnipresent deep level E3 in ZnO in detail. The E3 defect has already been thoroughly investigated in bulk crystals and epitaxial thin films.^[16,19–58] There exist only a few DLTS studies on samples that do not contain the E3 defect level.^[58–60] Its microscopic origin has not yet been definitively determined. First we will summarize

Dr. R. Pickenhain, Dr. H. von Wenckstern, G. Benndorf, Prof. A. Pöpl, Prof. R. Böttcher, Prof. M. Grundmann
Universität Leipzig
Felix-Bloch-Institut für Festkörperphysik
Linnéstraße 5, 04103 Leipzig, Germany
E-mail: wenckst@uni-leipzig.de

Dr. M. Schmidt
Helmholtz-Zentrum für Umweltforschung GmbH
Abteilung Isotopenbiogeochemie
Permoserstraße 15, 04318 Leipzig, Germany

 The ORCID identification number(s) for the author(s) of this article can be found under <https://doi.org/10.1002/pssb.201700670>.

DOI: 10.1002/pssb.201700670

the discussion of E3 in the literature. E3 is characterized by a thermal activation energy $E_c - E_t$ of from 260 to 310 meV and an apparent electron capture cross-section between 10^{-14} and 10^{-17} cm².^[16,19–58] The E3 concentration takes values up to 20% of the net doping concentration. There has been much speculation about its chemical origin. Besides the intrinsic donor-like oxygen vacancy and zinc interstitial defects, possible candidates include transition metals on the zinc lattice sites. Indeed, Jiang et al.^[27] detected, by EPR, iron and nickel in hydrothermally grown n-type ZnO bulk crystals, having irradiated the sample at low temperatures with a wavelength of 325 nm to transfer the transition metal ions X to the divalent X^{2+} state. During warm-up, the ions transfer back to the trivalent state X^{3+} with thermal activation energies of 240 meV for Fe^{2+} and 280 meV for Ni^{2+} .^[27] Schmidt et al.^[46] showed later that a nickel related state in ZnO had a higher thermal activation energy than E3. Vines and co-workers studied the behavior of E3 in hydrothermal bulk material upon thermal annealing and compared it to the amount of impurities within the samples after each annealing step.^[39,41] No correlation between the concentration of E3 and the concentrations of Al, Si, Mg, Fe, Mn, or Ni was observed, and it was concluded that E3 is very likely an intrinsic defect. A study of ZnO thin films annealed in argon, nitrogen, oxygen, and vacuum was published by von Wenckstern et al.^[36] revealing a decrease of the E3 concentration independently of the annealing atmosphere, which was interpreted as an argument against the intrinsic nature of E3. Another annealing study, of Quemener et al.,^[43] on hydrothermally grown bulk ZnO indicated that the E3 concentration was reduced by a factor of five if the annealing is done in an oxygen atmosphere, whereas no decrease of the E3 concentration was observed if the annealing took place in argon, nitrogen, or a nitrogen/hydrogen mixture of 90/10. They conclude that the E3 concentration is connected to an oxygen deficiency. In a later study of Quemener et al.,^[50] it was shown that the E3 concentration does not change due to annealing in either an oxygen or a zinc atmosphere in case the sample was annealed in argon atmosphere first. Mtangi and co-workers have found that the concentration^[51,52] and the defect parameters^[54] of E3 in melt-grown (MG) bulk material change after annealing in various gas atmospheres.

The creation/diminishing of defects due to implantation/irradiation with protons has been investigated.^[21,23,25,31,48,57] The E3 concentration did not change, with the exception of the study of Hupfer et al.,^[57] in which an increase of the E3 concentration was observed after proton implantation in hydrothermal bulk ZnO. Interestingly, implantation of helium ions does not change the concentration of E3^[57] and it is concluded that hydrogen must be involved in the E3 defect state. Oxygen implantation (500 keV O^+ ions) in hydrothermal and melt-grown ZnO bulk samples was performed by Vines et al.^[45] and revealed that the E3 concentration increases for low oxygen fluence (6×10^{11} cm⁻²), whereas a decrease is found for high fluences (2×10^{13} cm⁻²). The implantation of zinc ions does not change the E3 concentration in HT bulk ZnO.^[49] The same result was reported for ZnO thin films: the implantation of zinc^[38] or nickel ions^[46] had no impact on the E3 defect density. Gu et al. reported an increase of the E3 concentration in MG bulk ZnO samples after nitrogen ion implantation.^[35] After a subsequent annealing step at 1200 °C, the E3 density dropped below the detection limit.

Irradiation of ZnO with 170 keV electrons leads to an increase of the E3 density, whereas a reduction of the E3 density was reported after irradiation with 2 MeV electrons.^[29] A hydrogen plasma treatment of Zn-face ZnO shifts the DLTS peak temperature of E3 to higher values, as reported by Dong et al.^[40] Scheffler and co-workers performed hydrogen plasma treatments on ZnO thin films grown by chemical vapor transport (CVT) as well as hydrothermally grown (HT) and MG bulk ZnO material.^[47] In CVT thin films, the defect E3 was not detected. After the hydrogen plasma treatment the bulk samples underwent an additional annealing in oxygen or argon. The density of the E3 defect increases (decreases) if the annealing atmosphere was argon (oxygen), which led to the conclusion that E3 is a complex involving hydrogen.

In summary, very different and contradictory interpretations of the nature of the E3 defect in ZnO have been published. For its microscopic origin, transition metal ions,^[27,36] the oxygen vacancy,^[22,24] complexes involving the oxygen vacancy,^[40,55] hydrogen,^[47,57] and interstitial zinc,^[21,26,32] have been proposed, but a definitive judgement cannot be made so far. Therefore it is necessary to investigate the problem in more detail and determine and analyze the physical properties of E3 not yet described.

Not only the thermal activation energy but also the cross-section for electron capture of the E3 defect is of particular interest. Temperature dependent measurements of σ_n exist but even a reliable determination of the high-temperature limit σ_n^∞ (this is the apparent capture cross-section commonly determined in DLTS measurements) was impossible, which, most likely, is connected to a high charge carrier density in the particular samples (Ref. ^[16]). It can, however, be stated that σ_n^∞ is only weakly dependent on the electric field strength.^[24,55] This, together with σ_n^∞ being comparatively small ($\approx 2 \times 10^{-16}$ cm²), suggests that E3 is either neutral or negatively charged prior to electron capture.^[24,55] Chicot et al. conclude further that the defect potential of E3 must be asymmetric^[55]

To resolve the “E3-puzzle,” the optical properties of the defect are also of interest and will provide further information about the nature of the defect. In an earlier study from our laboratory by Ellguth et al.,^[19] it was found that E3 in ZnO thin films could not be photo-ionized. At that time, our system did not allow measuring defect emission rates smaller than $1s^{-1}$. In the meantime, our system has been improved, so that defect emission rates as small as $10^{-4}s^{-1}$ have become experimentally accessible.^[16] This now allows the determination of the optical properties of E3 in dependence on the sample temperature, photon energy, and photon flux. The extension of the detectable emission rates has of course also consequences for recording thermal DLTS spectra, allowing the detection of much deeper states. These very deep states have, in some cases, very high concentrations, even higher than the free electron density, so that their influence on the electrical properties of ZnO are crucial. This may in part explain the controversial interpretation of the nature of E3.

2. Experimental Section

We have characterized the properties of the deep level defect E3 in several earlier investigations.^[16,19,28,33,36,38,42,46,48,53,56,63,82] In

these experiments bulk samples obtained from *Tokyo Denpa* as well as heteroepitaxial thin films grown by pulsed laser deposition were used. Overall, about a hundred samples containing the E3 center were and are available. For the majority of these samples, ODLTS measurements are not conclusive since the deep defects labeled T4 and TH1 in the literature^[16] overlap with the E3 signal such that an unambiguous deconvolution of the ODLTS signal is impossible. Single crystalline bulk samples grown by the hydrothermal method are to our experience suited best for ODLTS investigations of E3 since the only deep level defect observable by DLTS is the E3 defect having high concentration, additionally. Overall, four nominally identical of such single crystalline samples ($10 \times 10 \times 0.5 \text{ mm}^3$) were used for this study. One of those crystals was used for investigations by photoluminescence and electron paramagnetic resonance measurements. On each of the other three samples about 30 circular Schottky barrier contacts were fabricated. For that, 40nm-thick AgO Schottky contacts were sputter-deposited in the center of a ring-shaped Ti/Al/Pt layer stack serving as an ohmic contact.^[61] The net doping density N_D was determined to be 10^{17} cm^{-3} by capacitance–voltage (CV) measurements. The samples were mounted on TO-20 sockets into which a hole was drilled so that the samples could be illuminated from the back-surface during the optical space-charge spectroscopic measurements. Using this geometry, the absorption of light at the Schottky contacts could be avoided.

The space-charge spectroscopy setup that we used consists of a He-flow cryostat suitable for the temperature range $4 \text{ K} < T < 400 \text{ K}$. The cryostat is equipped with LiF windows through which light can shine onto the sample. The light source in the experiments was a 100 W tungsten halogen lamp. The light was passed through a Carl Zeiss Jena SPM2 LiF prism-monochromator. This allows for an illumination of the sample with a monochromatic photon flux $\Phi(h\nu)$ in the spectral range of $250 \text{ meV} < h\nu < 4000 \text{ meV}$. The deep-level transient spectroscopy measurements were conducted using a home-built capacitance bridge controlled by in-house coded software. This allows for the recording of capacitance transients of arbitrary duration, with up to 10^5 sampling points in dependence on the temperature and/or photon flux and energy. The minimum pulse width of the system is 500 ns. The setup is described in detail in Ref. ^[16].

Photoluminescence (PL) measurements were carried out in dependence on the temperature in a helium flow cryostat. The samples were excited with an excitation density of about 0.2 W/cm^2 using the 325 nm line of a CW He-Cd laser. Moreover, various semiconductor diode lasers (Roithner LaserTechnik GmbH) were used with wavelengths of 405 nm (50 mW, RLDE405-50-5), 450 nm (40 mW, RLDD450-40-5), 520 nm (5 mW) and 980 nm (50 mW, LDM-0980-050-50). The sample luminescence was spectrally dispersed by a monochromator Jobin Yvon HR320 with a focal length of $f = 320 \text{ nm}$ using a $150 \text{ grooves mm}^{-1}$ grating. The detector was a cooled Jobin Yvon back-illuminated CCD with 2048×512 pixels.

Electron paramagnetic resonance (EPR) experiments were performed using a Bruker EMX micro spectrometer at X-band frequencies (microwave frequency $\nu_{\text{mw}} = 9.456 \text{ GHz}$) using a cylindrical ER4191HS cavity mounted in an Oxford Instruments ESR900 flow cryostat. The ZnO single crystal was mounted on a

quartz rod sample holder. The angle between the *c*-axis of the crystal and the direction of the applied magnetic field was controlled by a goniometer.

3. DLTS Measurements

Deep Level Transient Spectroscopy (DLTS)^[62] and Optical Deep Level Transient Spectroscopy (ODLTS)^[17] are both based on the investigation of carrier emission from defect levels within the bandgap of semiconductors. The thermal emission rates of electrons and holes are given by^[65]

$$e_{n,p}^{\text{th}} = \sigma_{n,p}^{\infty} \langle v^{\text{th}} \rangle_{n,p} N_{c,v} \exp\left(-\frac{\Delta H}{k_B T}\right) \exp\left(\frac{\Delta S}{k_B}\right) \exp\left(\frac{-E_{n,p}^{\infty}}{k_B T}\right). \quad (1)$$

Thereby $N_{c,v}$ is the effective density of states in the conduction and valence band, ΔH and ΔS the enthalpy and entropy change due to the transition, $\sigma_{n,p}^{\infty}$ the defect's capture cross-section at infinite temperature, respectively, and $E_{n,p}^{\infty}$ the thermal capture barrier for electrons and holes. With that the apparent capture cross-section $\sigma_{n,p}$ can be written as

$$\sigma_{n,p} = \sigma_{n,p}^{\infty} \exp\left(\frac{\Delta S}{k_B}\right) \exp\left(\frac{-E_{n,p}^{\infty}}{k_B T}\right). \quad (2)$$

By evaluating the entropy changes ΔS one finds the probability that the trap is occupied and with that the thermal emission rates to be

$$e_{n,p}^{\text{th}} = \sigma_{n,p} \langle v^{\text{th}} \rangle_{n,p} N_{c,v} \exp\left(\pm \frac{E_{c,v} - E_t}{k_B T}\right). \quad (3)$$

$E_{c,v}$ denoting the energy position of the conduction and valence band edge, E_t denotes the thermal activation energy of the deep level. The emission rates of an optical emission process are given by Brehme et al.^[17]

$$e_{n,p}^{\text{o}}(h\nu) = \sigma_{n,p}^{\text{o}}(h\nu) \times \Phi(h\nu), \quad (4)$$

where $\sigma_n^{\text{o}}(h\nu)$ denotes the photon energy dependent photo-ionization cross-section for the optical emission of electrons trapped in E3 into the conduction band. The emission e_{rate} of electrons from a deep defect is then the sum of a thermal and optical emission

$$e_{\text{rate}} = e_{n,p}^{\text{th}} + e_{n,p}^{\text{o}}(h\nu). \quad (5)$$

If the concentration N_t is constant for the deep defect in the space charge region and if $N_t < N_D$ the concentration of the deep defect N_t can be written as^[65]

$$N_t \approx \frac{\Delta C}{C} 2 \times N_D, \quad (6)$$

C is the capacitance of the sample at given temperature and $\Phi(h\nu)$.

DLTS measurements on HT grown ZnO single crystals were performed in the temperature range $50 \text{ K} < T < 400 \text{ K}$. This

temperature range is given by the freeze-out of the mobile charge carriers below 50 K and the degradation of the Schottky contacts above 450 K. For emission rates of $9 \times 10^{-4} \text{ s}^{-1} < e_{\text{rate}} < 4200 \text{ s}^{-1}$ exclusively the deep level E3 in a concentration of approximately 20% of the net doping density was revealed. The concentration of E3 varies only slightly among the samples. These samples are therefore excellently suited for studying the properties of E3 as already stated above.

In **Figure 1** the DLTS signal of E3 is depicted. A straight line fit of the Arrhenius plot of the temperature dependence of the thermal emission rate of E3, inset of Figure 1, determines the thermal activation energy of this deep level as $E_t = 280 \text{ meV}$ and its apparent electron capture cross-section as $\sigma_n^\infty = 2.2 \times 10^{-17} \text{ cm}^2$. If small emission rates $< 0.5 \text{ s}^{-1}$ are employed, the DLTS signal maximum decreases with decreasing emission rates. This is due to the exponential temperature dependence of the electron capture cross-section of E3,^[63] which becomes noticeably smaller for $T < 150 \text{ K}$. In turn, the thermal electron capture rate decreases tremendously and becomes comparable to the electron emission rate e_n^{th} , so that the concentration of the deep level is underestimated. Furthermore, a constant DLTS signal is observed for emission rates smaller than 0.001 s^{-1} . This might be due to tunneling emission of electrons from E3 into the conduction band. Double DLTS measurements revealed that the E3 defect concentration is homogeneous (within the accessible space charge region width of $w \leq 1 \mu\text{m}$).

In **Figure 2** the ODLTS($h\nu, T = 80 \text{ K}$) signal of E3 measured at 80 K is depicted. The measurement was carried out for a range of emission rates $9 \times 10^{-4} \text{ s}^{-1} < e_{\text{rate}} < 4 \text{ s}^{-1}$ and the photon energy was varied over the range $450 \text{ meV} < h\nu < E_g$. The ODLTS($h\nu, T = 80 \text{ K}$) measurement was conducted in such a way that the voltage pulses filled the deep levels, as was also done for the thermal DLTS. After the filling pulse, the sample was reverse biased, and light shone from the backside through the sample onto the Schottky contact.

At 80 K almost no thermal ionization of E3 occurs, $e_n^{\text{th}} < 10^{-6} \text{ s}^{-1}$. Hence, Eq. (5) reduces to $e_{\text{rate}} = e_n^o(h\nu)$. In order to determine the optical emission rates $e_n^o(h\nu)$ correctly from the ODLTS($h\nu, T = 80 \text{ K}$) signal, the maximum of the ODLTS

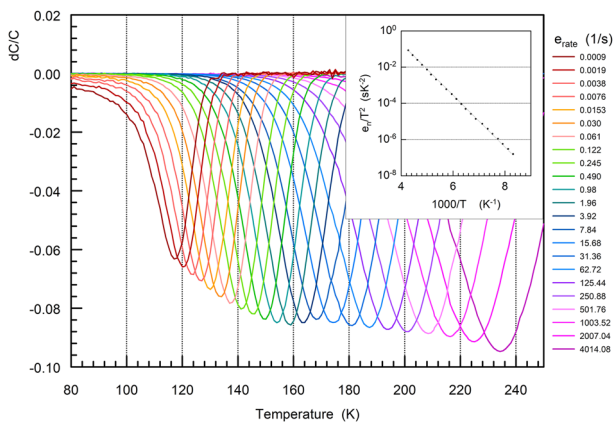


Figure 1. DLTS-scan of the E3 with different emission rates. $U_r = -3 \text{ V}$, the filling pulse amplitude is 3 V and the pulse time is 0.1 s. The Arrhenius plot is represented in the inset.

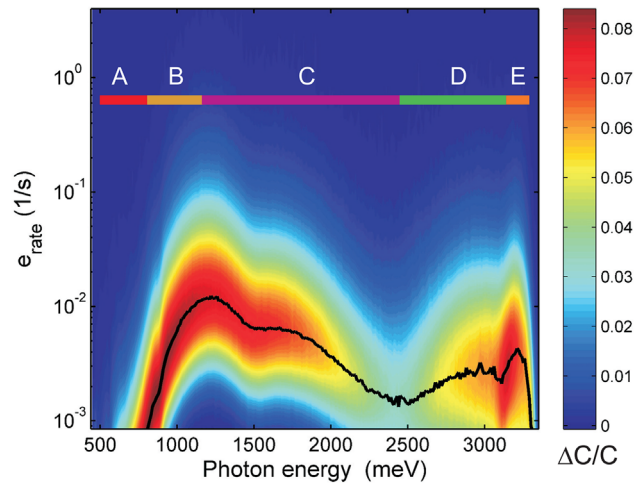


Figure 2. ODLTS($h\nu, T = 80 \text{ K}$)-scan of E3 at 80 K. The ODLTS signal $\Delta C/C$ is shown in false colors in dependence on photon energy and optical emission rate. The black line indicates the maximum $S(h\nu, e_{\text{rate}})$ of the ODLTS signal. The spectral regions A–E are discussed in the text.

($h\nu, T = 80 \text{ K}$) signal needs to be determined. The dependence of this maximum ODLTS($h\nu, T = 80 \text{ K}$) peak height $S(h\nu)$ (black line in Figure 2) in dependence on the photon energy is depicted in **Figure 3**. The onset of the optical emission occurs at $h\nu \approx 550 \text{ meV}$ (Figure 2) which in turn is the threshold energy for the photo-ionization cross-section $\sigma_n^o(h\nu)$. Within the range $550 \text{ meV} < h\nu < 800 \text{ meV}$ (region A), even the smallest emission rate e_{rate} measured in this research did not allow reaching the ODLTS($h\nu, T = 80 \text{ K}$) signal maximum. However, following Goto et al.,^[64] $e_n^o(h\nu)$ was determined using the inverted DLTS correlation function. For $h\nu > 800 \text{ meV}$ the ODLTS($h\nu, T = 80 \text{ K}$) signal maximum is reached (region B to E) and $e_n^o(h\nu)$ can be directly determined from the e_{rate} at which the maximum occurs. The ODLTS signal maximum of a deep level interacting with one band only (conduction band or valence band) should not increase with increasing photon energy, because within this maximum $\Delta C/C$ corresponds to the concentration of the deep level. For $h\nu > 1000 \text{ meV}$, the ODLTS($h\nu, T = 80 \text{ K}$) signal maximum continuously drops with increasing photon energy (region C) with a minimum at $h\nu \approx 2450 \text{ meV}$. Beyond that energy, it rises again

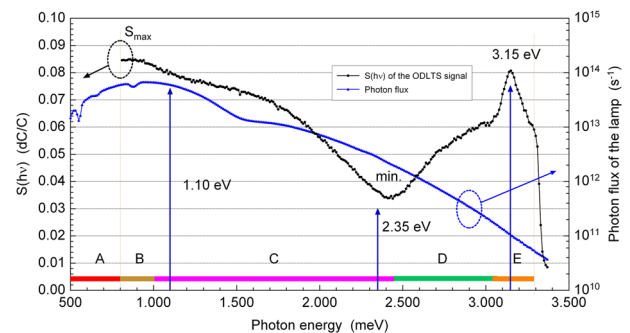


Figure 3. The signal maximum $S(h\nu)$ of the ODLTS($h\nu, T = 80 \text{ K}$)-scan (same as black line in Figure 2) as a function of the photon energy at 80 K. Spectral regions A–E are discussed in the text.

(D) and reaches almost the initial maximum peak height, within the range (E).

The question arises whether the ODLTS($h\nu, T=80$ K) signal measured in these experiments stems exclusively from E3 or if other deep levels contribute to the signal? DLTS signals of different deep level defects are additive. Further, each defect level has characteristic thermal and optical emission rates.^[65] For the measurement conditions of Figure 2 electrons are emitted from the deep level by optical excitation. If the temperature increased such that $e_n^o \ll e_n^{th}$ Eq. (5) reduce to $e_{rate} = e_n^{th}$ and the DLTS signal will be dominated by thermal emission of electrons from the deep level. Now, if k different deep level defects, each having characteristic activation energy and capture cross-section, were present, then each deep level defect has a characteristic temperature T_k for which $e_n^o \sim e_n^{th}$ holds (for a given photon flux).

In order to answer this question, DLTS measurements with additional illumination, $h\nu = (1100, 2350, 3150)$ meV, were conducted. The results are depicted in **Figure 4** and show that an optical emission is detectable only if the thermal emission rate e_n^{th} of E3 is smaller than the measured optical emission rate e_n^o . We find that the condition $e_n^{th} \sim e_n^o$ is for each photon energy fulfilled at the same temperature. This proves that undoubtedly for $h\nu < 3200$ meV the optical emission stems exclusively from the optical emission of electrons bound to E3.

According to Jaros,^[66] $\sigma_n^o(h\nu)$ is proportional to the electronic transition probability from the state localized at the deep-level defect into the continuum of conduction band states. The transition matrix elements were calculated by Lucovsky^[67] assuming δ -type potentials for the deep-level state. These results were used by Chantre et al.^[18] for constructing configuration-coordinate diagrams of several deep-level centers in GaAs from DLOS measurements. We have applied the model to the ODLTS data of E3. However, a physically meaningful set of parameters for a configuration-coordinate diagram could not be derived. The finding that the model of Lucovsky is not applicable to the E3

defect in ZnO is in line with Chicot et al.,^[55] who assigned an asymmetric potential to E3.

In order to calculate the photo-cross section $\sigma_{n,p}^o(h\nu)$ of the E3 defect with Eq. (4), the optical emission rate $e_n^o(h\nu)$ has to be determined for each $h\nu$ and given photon flux $\Phi(h\nu)$ from the maximum of the DLTS signal. Let us revisit the ODLTS maximum signal $S(h\nu)$ as depicted in Figures 2 and 3. The highest values of the ODLTS maximum are observed in region B, but this value is smaller than the signal height of the thermal DLTS signal observed at 200 K (cf. Figure 1). The decrease of the thermal DLTS signal for the smallest emission rate e_n^{th} was already discussed and explained by incomplete filling. Hence the height of the thermal DLTS signal does not correspond to the E3 defect concentration for these small emission rates. In order to determine the true concentration of the E3 defect, temperature dependent capacitance $C(T)$ measurements^[68] were carried out in the temperature range from 50 to 180 K both under dark conditions and under optical excitation. The results are depicted in **Figure 5**. Prior to the temperature scans under 3V reverse bias, the initial state of the E3 defect within the bulk of the depletion layer was prepared by a reverse voltage applied during cooling. The state is not occupied if the sample is cooled under a reverse voltage of 3V (curve (a) in Figure 5) and it is fully occupied if the sample is cooled under zero bias (curve (b) in Figure 5). The capacitance differences in the experiments (a), E3 totally empty, and (b), E3 completely occupied, between about 70 and 110 K, represent the concentration of E3 within the bulk of the depletion layer. The concentration of E3 defect can be calculated using Eq. (6). At a temperature of 80 K the concentration of the E3 defect is $N_t = 0.24 \times N_D$, which is slightly higher than the value of $N_t \approx 0.18 \times N_D$ determined from the DLTS measurement but reflects the true value of the E3 concentration. The freeze-out of free carriers occurs for temperatures below 60 K as depicted in the inset of Figure 5.

Experiment (c) was conducted identically to curve (b) but with additional optical excitation with 1.1 eV photons. Electrons are optically emitted from the E3 defect. The optical excitation leads to somewhat different measurement conditions. Besides the occupation of E3 by electrons, also the occupation of shallower and deeper states is influenced, and changes the space charge width upon irradiation. Line (c) is representative for illumination with photon energies smaller 1.1 eV. The photon irradiation does obviously not cover the entire space charge region and hence the capacitance is slightly lower compared to case (a) for which the E3 defect levels within the entire depletion region were unoccupied. For this reason we use the curve labeled (c) as reference for the $C(T)$ measurements with optical excitation.

If the sample is illuminated with 2.35 eV photons (experiment e), the capacitance is exactly in the middle between experiments (c) and (b) (curve d). In other words, the minimum occupancy of the E3 deep levels in the space charge region under 2.35 eV illumination is no less than one-half the maximum occupancy. Therefore the $C(T)$ measurements are in accordance with the ODLTS measurements of Figures 2 and 3. In addition, we can conclude that the minimum ODLTS

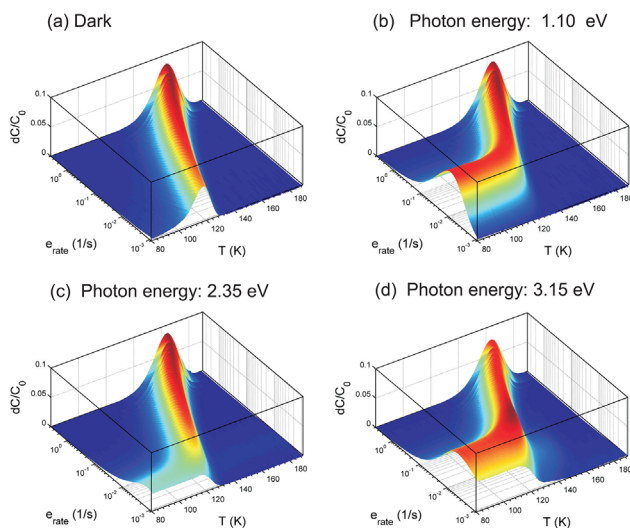


Figure 4. ODLTS($h\nu = \text{const}, T$)-scans of the E3 at a temperature of 80 K and with different photon energies.

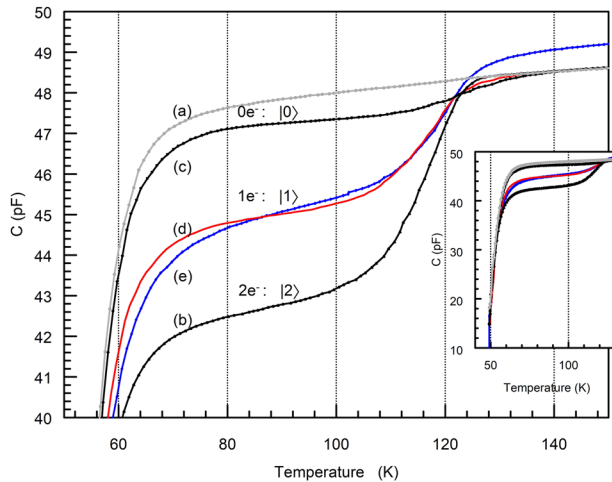


Figure 5. Temperature dependent capacitance of the ZnO sample measured in the dark and under different illumination schemes (see text). Curve (d) is constructed as $((c) + (b))/2$. The changes are due to the different charge states of E3. Freeze-out of free carriers occurs for temperatures lower than 60 K as visible in the inset of the figure.

signal height for $h\nu = 2.35$ eV is greater than or equal to $N_t/2$.

We ascertain that the mean electron occupation of the E3 defect under optical excitation is depending on the photon energy and lies between $N_t/2$ and N_t .

The question is now, what is the origin of the decrease of the ODLTS signal maximum beyond $h\nu > 1000$ meV (Figures 2–4) and of the unusual result of the $C(T)$ measurement for these photon energies? There has to be an optical emission process, which first lowers the mean occupancy of E3 with electrons with increasing photon energy (as of $h\nu \approx 1000$ meV) and then, beyond $h\nu \approx 2450$ meV, allows it to increase again. A refilling by valence band electrons would involve an unlikely three-photon process. Further, the defect would have to have two additional states with a respective energetic spacing of 1 eV and thus this process is ruled out. Further it can be ruled out that these defect states originate from defects other than the E3 defect, since the optical properties of the E3 defect were independent of the investigated sample, even though the E3 concentration and the concentration of other defects differed significantly. If defects other than E3 were involved in the refilling of E3, their concentration would have to scale with that of E3. This again is, due to the different growth processes of the samples, highly unlikely. In addition, transitions different from that with E3 as the final state should be visible in the ODLTS measurements, which is not the case. Also according to first-principles calculations, intrinsic defects with three transition levels do not exist (Janotti et al.^[69]).

This implies that a model involving a singly chargeable E3 defect is not capable of explaining our experimental results. A more complex model is required to explain the properties of the E3 defect level. Based on the ODLTS and the $C(T)$ measurements, we therefore conclude that the E3 defect can bind two electrons. Further, E3 must be considered as a negative- U center since the experimental results do not conform with those of a positive- U defect.

The emission rates of the possible optical transitions are e_{21}^o , e_{20}^o , and e_{10}^o , as depicted in Figure 6. The capture rates can be neglected since free carriers are not present within the space charge region during transient acquisition. The time evolution of the occupation of E3 by electrons under optical excitation is given by the differential equations

$$\begin{aligned} \frac{dq_2}{dt} &= -(e_{21}^o + e_{20}^o)q_2 \\ \frac{dq_1}{dt} &= -e_{10}^oq_1 + e_{21}^oq_2 \end{aligned} \quad (7)$$

and the solution is provided by Eq. (13) of the Appendix. q_1 and q_2 are the probabilities of finding the defect occupied by 1 or 2 electrons, respectively. The probability that the defect is empty, q_0 , can be calculated from $1 = q_0 + q_1 + q_2$. For photon energies $h\nu < 1.0$ eV we find $e_{21}^o = e_{10}^o = 0$ and from Eq. (15) follows $Q(t) = 2(1 - e^{-e_{20}^ot})$. The E3 defect behaves for $h\nu < 1.0$ eV like a common deep-level defect, but two electrons are emitted during the transition from state $|2\rangle$ to state $|0\rangle$.

For photon energies $1\text{ eV} < h\nu < 2.35\text{ eV}$ only $e_{10}^o = 0$ at 80 K and we find Eq. (16) as the solution of Eq. (7). Depending on the value of e_{21}^o , electrons may now be transferred from the state $|2\rangle$ into the conduction band or to the state $|1\rangle$. Consequently a reduction of the maximum ODLTS signal height is observed since not both of the electrons that occupied the E3 state are emitted into the conduction band. The electron that was transferred to state $|1\rangle$ cannot be emitted either thermally or optically, and remains trapped. In other words, state $|1\rangle$ lies lower in the band gap than state $|2\rangle$. This can be explained by a strong lattice relaxation around the defect center and implies that E3 is a negative- U center.^[70,65] The reduction of the capacitance step height, observed in the $C(T)$ measurements for $1\text{ eV} < h\nu < 2.35$ eV, is then also due to the filling of state $|1\rangle$. Neither a thermal nor optical emission is possible at 80 K from $|1\rangle$. For this case the solution of the differential equation is given by Eq. (23), which can be used to calculate from the experimentally determined parameters $S(e_{20}^o/e_{21}^o)$, S_{\max} (cf. Figure 3) and the emission rate e_{20}^o at the DLTS signal maximum the emission rates e_{21}^o and e_{20}^o of E3 in dependence on the photon energy. The photo-ionization cross-sections $\sigma_{20}(h\nu)$ and $\sigma_{21}(h\nu)$ are now obtained by applying Eq. (4) and are depicted in Figure 7. As already obvious from Eq. (23), e_{20}^o is virtually zero for photon energies around 2.4 eV. The DLTS signal is then due to the transition $|2\rangle \rightarrow |1\rangle$. For photon energies $h\nu > 2.4$ eV the emission rate $e_{10}^o \neq 0$ and Eq. (25) must be used for the evaluation. In this case there are three unknowns but only two measured parameters. Hence, additional assumptions have to be made. Further, the DLTS signal is now composed of two terms

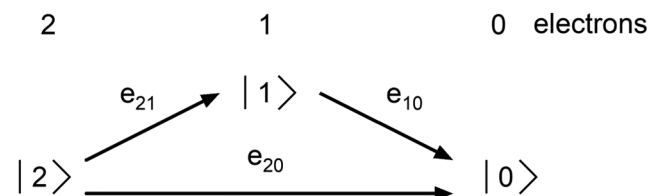


Figure 6. Emission rates in the two-electron model.

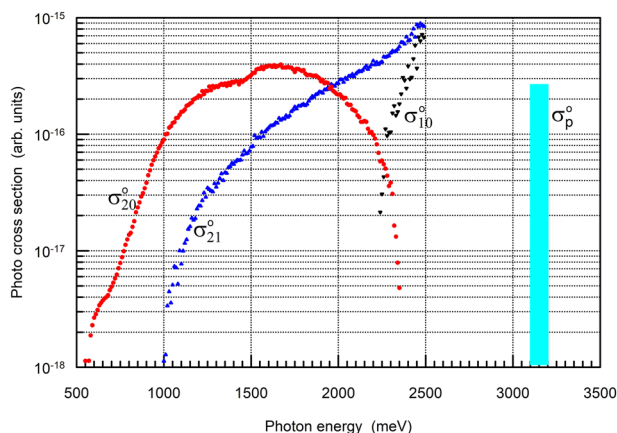


Figure 7. Photo-ionization cross-sections of E3 calculated for $T = 80$ K using Eq. (7). σ_p^o indicates energies for which electrons from the valence band are transferred into E3 (region E in Figures 2 and 3).

having different transient decay times. In order to evaluate the transients, we assume that $e_{20}^o = 0$ for $h\nu > 2.4$ eV. The difference between the emission rate at the signal maximum and the calculated value of $\sigma_{21}^o(h\nu)$ can be used to determine the initial behavior of e_{10}^o . Besides $\sigma_{20}^o(h\nu)$, $\sigma_{21}^o(h\nu)$, and $\sigma_{10}^o(h\nu)$, a peak at 3.15 eV is visible in Figures 2 and 3 and is obviously due to the transition of electrons from the valence band to the E3 defect level. The parameters connected to this transition are labelled e_p^o and σ_p^o from now on.

4. Photoluminescence

DLTS measurements provide information on capture processes and the concentration of a deep level defect. Additional information on deep level defects can be obtained from photoluminescence measurements. For samples with high E3 defect concentration we always observe a broad green luminescence band and suppose a connection between this luminescence band and the E3 defect level. For this purpose, the sample can first be excited above the band gap. Besides the near band edge emission (NBE), a broad emission band centered at 2.27 eV with a full width at half maximum (FWHM) of about 600 meV is observed at room temperature (RT) and depicted in **Figure 8(i)**. The broad emission can be well fitted by a Gaussian distribution. If the band belongs to a single transition, it has a strong electron–phonon coupling with a Huang–Rhys factor $S > 8$ (Ref. [65]).

Broad luminescence bands in the visible spectral range have been discussed in the literature.^[1,71–73] Seto et al. found such a green luminescence band in HT single crystals grown by Tokyo Denpa.^[74] In the following we present investigations of the green emission band and establish a connection between this luminescence and the E3 defect.

If sub-band gap illumination with $\lambda = 405$ nm (3.06 eV) is used, we would not expect any photoluminescence. However, a broad luminescence band is detected. The wavelength of the laser $\lambda = 405$ nm (3.06 eV) is such that it is within the spectral region E of Figures 2 and 3 or at σ_p as shown in Figure 7.

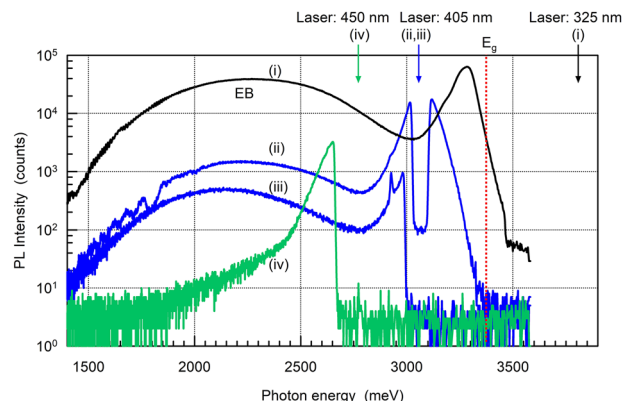


Figure 8. Photoluminescence under different excitations at $T = 300$ K: (i) 325 nm excitation with 355 nm edge filter. (ii) 405 nm excitation and 405 nm notch filter. (iii) 405 nm excitation and 409 nm edge filter. (iv) 450 nm excitation and 458 nm edge filter.

The luminescence is measured with a 405 nm notch filter (**Figure 8(ii)**) and a Raman long pass edge filter for 409 nm (**Figure 8(iii)**) placed in front of the monochromator. The broad emission band is visible even though only sub-band gap excitation is used. Since the E3 defect is not occupied by electrons at RT, these can be transferred from the valence band to E3 by an optical transition. Subsequently these electrons recombine with valence band holes, resulting in the broad emission band. Next the sample is excited with $\lambda = 450$ nm (2.75 eV) and a Raman long pass edge filter for 458 nm (**Figure 8(iv)**) such that a transition of valence band electrons into E3 is not possible. In this case, the broad emission band is no longer observed and we conclude that this emission band is directly connected to the existence of the E3 defect in ZnO. Further evidence for the connection of the broad band to the E3 center is obtained from photoluminescence measurements acquired at temperatures ranging from 80 to 220 K, as depicted in **Figure 9**. The mean occupation of E3 by electrons is reduced if the temperature is increased. At 80 K and excitation with $\lambda = 405$ nm, the broad emission band has a much lower intensity compared to the RT measurement. At 3 eV we observe a Raman line and residual laser light.

The maximum intensity is observed at 2.09 eV. This lower intensity is explained by the occupation of E3 by electrons; an excitation of valence band electrons into E3 is not possible, which further implies that none of the free holes necessary for a radiative recombination of electrons occupying the E3 defect are generated. As the temperature is increased, the intensity of the broad emission band increases exponentially with T , as one expects from the temperature dependent activation of electrons from E3 to the conduction band, which means that electrons can be transferred from the valence band to these E3 centers creating holes in the valence band for radiative recombination. Hence, the intensity of the broad emission band is inversely proportional to the mean occupation of E3 by electrons. The peak energy position of maximum luminescence intensity remains at 2.09 eV.

A broad and intense emission band is observed if the sample is excited above the band gap with $\lambda = 325$ nm. The maximum

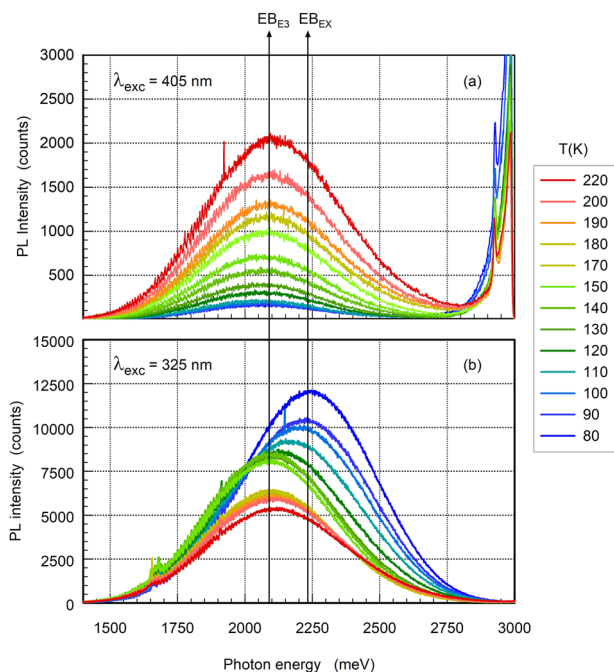


Figure 9. Photoluminescence intensity under different temperatures. (a) 405 nm excitation. (b) 325 nm excitation.

intensity occurs at a higher energy (2.23 eV), as can be seen in Figure 9b. Now, electrons are excited from the valence into the conduction band. The free holes created in the valence band can now recombine with electrons located at the E3 defect. The energy of maximum intensity is higher compared to the sub-band gap excitation, which indicates that a second recombination process exists that requires conduction band electrons. The overall intensity of the broad emission band decreases with increasing temperature and the energy of maximum intensity gradually shifts to 2.09 eV. In contrast to the sub-bandgap excitation with the 405 nm laser, excitation with the 325 nm laser creates a high density of free holes in the valence band. Therefore, the PL signal at 2.09 eV will not vanish for temperatures of 80 K and below.

To summarize, the broad emission band is composed of two recombination processes, one of them (labelled EB_{E3}) has its maximum recombination intensity at 2.09 eV, a full width at half maximum (FWHM) of about 500 meV and increases in intensity proportionally to the thermal emission of electrons from E3 to the conduction band. The second process (labelled EB_{EX}) has its maximum intensity at 2.23 eV, a FWHM of about 600 meV, and is visible only for $T < 150 \text{ K}$ and excitation above the band gap. The temperature dependence of the EB_{EX} signal requires clarification.

The deep-level defect E3 is connected to the optical transition with highest intensity at 2.09 eV (593 nm). The temperature dependence of the intensity of the broad emission band has already been investigated, for example, by Seto et al.^[74] and Ahn et al.^[75]. However, no microscopic origin has been assigned to this emission band. This may be partly due to the fact that with an excitation above the band gap, a separation of the unintentionally measured EB_{E3} transitions from other recombination channels

was not possible. Leiter et al.^[73] used optically detected magnetic resonance measurements to show that the green luminescence band in ZnO is connected to the oxygen vacancy. The ODMR experiments revealed a triplet spectrum of a center with a total electron spin $S = 1$ in the range of the green emission band at 2.45 eV with g values $g_{\text{zz}} = 1.984$, $g_{\text{xx,yy}} = 2.025$ and a fine structure parameter $D = 260 \times 10^{-4} \text{ cm}^{-1}$. This center has been assigned to the first excited triplet state of a neutral oxygen vacancy $\text{V}_{\text{O}}^{\times}$ which is occupied by two electrons. We did not observe a green emission band centered around 2.45 eV.

5. EPR Experiments

Electron paramagnetic resonance measurements were carried out on the ZnO single crystal to gain further information about the paramagnetic defects it contains. The measurements were performed at different temperatures and under optical excitation using solid state lasers with photon energies of 3.061, 2.755, 2.384, and 1.265 eV (405, 450, 520, and 980 nm). From measurements under dark conditions, the presence of Mn^{2+} ,^[76] Co^{2+} ,^[77] and Fe^{3+} ^[78] was determined. These impurities are not connected to the E3 defect, because the variation of temperature and/or photon energy should change the occupation of E3 and with that its EPR activity. The EPR signal of the Fe^{3+} center disappears upon illumination at low temperatures as reported by Evans et al.^[79] whereas the EPR signal of Mn^{2+} appears to be independent of the illumination at any measuring temperature. Due to relaxation the Co^{2+} signal is visible only for low temperatures.

Further, we detected $\text{Li}^{[80]}$ and the signature of a shallow donor.^[7,81] The signal corresponding to Li_{Zn} is visible only after optical excitation, except for the 980 nm laser. At 80 K, only axial centers are created, but an illumination at 30 K generates non-axial centers as well. The g -factor of the axial center was determined to be $g_{\parallel} = 2.0033(3)$ and $g_{\perp} = 2.0255(3)$. The non-axial center has orthorhombic symmetry and its g -values are $g_{\text{xx}} = 2.0225(3)$ and $g_{\text{zz}} = 2.0040(3)$. As depicted in Figure 10, the signal of the non-axial (axial) center diminishes for $T > 65 \text{ K}$ ($T > 150 \text{ K}$). At RT, Li_{Zn} cannot be detected by EPR. This implies that E3 is not connected to Li_{Zn} since it also was observed in thin film samples that are not Li contaminated (e.g., in thin films grown by pulsed laser deposition^[16,19,28,36,38,42,46,48,53,56,63,82]). The EPR signal of the shallow donor is only observable after optical excitation (except for the 980 nm laser) and for $T \leq 80 \text{ K}$. The line width shows a strong temperature dependence (it is 0.9 G at 80 K and 4.3 G at 30 K). The g -factors of the shallow donor are $g_{\parallel} = 1.9568(3)$ and $g_{\perp} = 1.9960(3)$. The decrease of the EPR signal of the shallow donor starts at 60 K and corresponds well to the increase of the sample conductivity, which starts at 60 K as well.

Finally, a further narrow EPR signal with $g_{\parallel} = 1.9947(3)$ and $g_{\perp} = 1.9957(3)$ and a line width of 0.99(5) G of an axially symmetric defect center with electron spin $S = 1/2$ becomes visible upon optical excitation (except for the 980 nm), cf. Figure 11. The same signal has been observed for electron-irradiated (Refs. [79,83–86]) and non-irradiated (Ref. [14]) ZnO single crystals as well as in ZnO ceramics (Refs. [87,88]). Photo EPR experiments revealed a comparable optical response of the signal for the various materials.

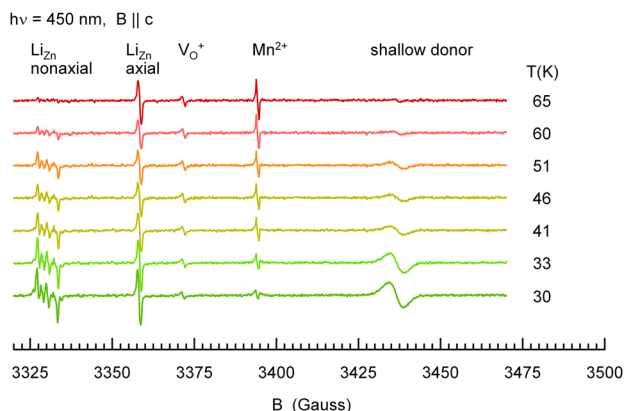


Figure 10. EPR spectra of the ZnO bulk crystal recorded under optical excitation with 3.061 eV photons for temperatures as labelled and $B \parallel [0001]$.

The signal occurs at photon energies larger than 1.8 ... 2.0 eV and peaks at about 2.5 ... 2.6 eV (Refs. [14,79,85–87]). Large signal intensities were obtained for electron-irradiated ZnO single crystals which enabled the detection of super hyperfine interactions (shfi) of the defect center with an axial and three non-axial next-neighbored ^{67}Zn nuclei.^[83,84,85] Based on the ^{67}Zn shfi the signal has been assigned to the singly positively charged oxygen vacancy V_{O}^+ (Ref. [83,84]).

If we compare the EPR results to the results obtained by space charge spectroscopy, the following has to be considered. EPR measurements are performed without the application of an electric field to the sample. Further, for $T > 60$ K, free electrons are in the conduction band and may occupy a state that optically emits an electron, instantaneously. The properties of the oxygen vacancy as determined by the EPR measurements and that of the E3 defect center have distinct similarities as detailed below.

- (a) The signal intensity of the oxygen vacancy is about two-tenth of that of the shallow donor and corresponds well to the ratio of the E3 defect density and the net doping density (Figure 5, inset) of the sample.

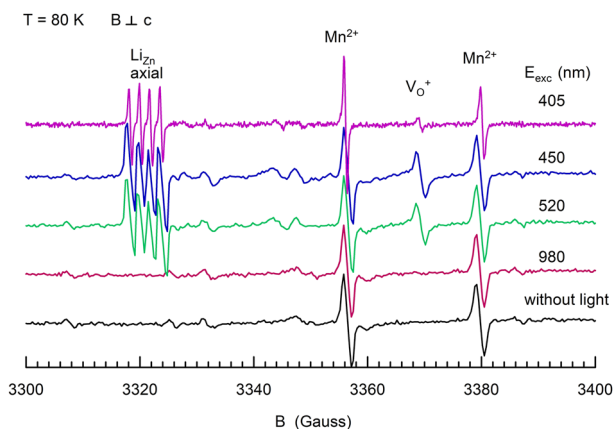


Figure 11. EPR spectra of the ZnO bulk crystal recorded at $T = 80$ K under illumination with photons of energies as labelled and $B \perp [0001]$.

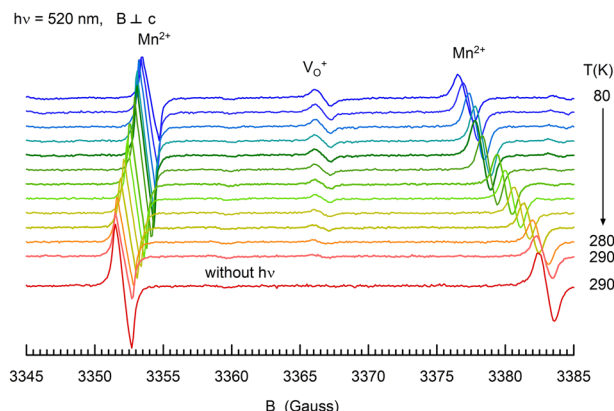


Figure 12. EPR spectra of the ZnO bulk crystal recorded under optical excitation with 2.348 eV photons for temperatures as labeled and $B \perp [0001]$.

- (b) For $T = 80$ K, the EPR signal of the oxygen vacancy V_{O}^+ remains even though the optical excitation is switched off and even though free electrons are available to occupy the defect state. The EPR signal diminishes only if the sample is heated under dark conditions to $T > 200$ K. This implies that the V_{O}^+ centers created at 80 K are stable after the light was switched off, which is in line with the properties of the E3 defect (cf. Figure 5). At RT, the V_{O}^+ signal decays (on a time scale of milliseconds) as soon as the optical excitation is turned off. Similar behavior is observed for E3.
- (c) The temperature dependence of the EPR intensity of the V_{O}^+ center is depicted in Figure 12. For the measurements we chose the microwave power such that the V_{O}^+ center was not saturated for any measuring temperature. Further the photon flux of the laser light is so high that the EPR signal intensity only depends on the number of V_{O}^+ centers; it is independent of the photon flux. Further, the quality factor of the sample/resonator system was determined for each temperature and was used to correct signal variation due to changes of the quality factor.^[89] This corrected EPR intensity of the V_{O}^+ center is depicted in Figure 13 in dependence on

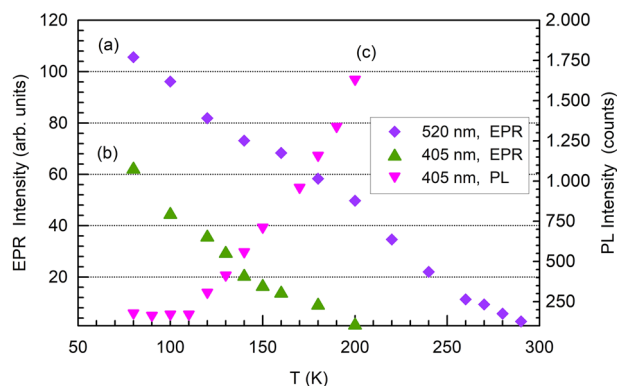


Figure 13. EPR intensity of the V_{O}^+ center and PL intensity for different temperatures. (a) EPR intensity for 520 nm excitation. (b) EPR intensity for 405 nm excitation. (c) PL intensity for 405 nm excitation.

the temperature and for irradiation with photons with 2.384 or 3.061 eV energy, respectively, and together with intensity of EB_{E3} emission band. The intensity of the EPR signals decreases for both cases with increasing temperature while the intensity of the EB_{E3} increases. The intensity decreases for both cases with increasing temperature. The most obvious explanation is the reduction of the number of V_O^+ centers with increasing temperature. Under dark conditions and for irradiation with photon energy below 1.265 eV the oxygen vacancy is occupied by two electrons and not EPR active (cf. Figure 11). If the sample is irradiated with photon energy above 2.384 eV, V_O^+ is excited into the EPR active state V_O^+ resulting in the temperature dependent EPR signal. The ODLTS measurements revealed that the single electron state of E3 is created for photon energies above 1 eV and that its generation is maximal for a photon energy of 2.35 eV. An increase in temperature diminishes the creation rate of E3 in the single electron state because more and more E3 centers are thermally excited from the two electron state into the unoccupied state. Hence, with increasing temperature the number of oxygen vacancies that can be transferred in the V_O^+ state is reducing.

- (d) The close resemblance between E3 center and the oxygen vacancy is substantiated by the temperature dependent EPR measurements with irradiation of photons with energy of 3.061 eV (cf. Figures 11 and 13). The intensity of the EPR signal is for this photon energy clearly lower as for irradiation with photon energy of 2.348 eV. Further, the signal already vanishes for $T > 200$ K instead of 300 K. From Figure 7 we see, that photon energy of 3.061 eV is sufficient to excite electrons from valence band into the $|2\rangle$ state of E3 (onset of σ_p^0). Optical excitation with photon energy resulted in the photoluminescence band EB_{E3} as well (cf. Figure 9a). The intensity of the EB_{E3} band increase with increasing temperature in such way as the EPR signal of V_O^+ decreases because the recombination channel via EB_{E3} results in a decrease of the mean electron occupation of the E3 center. Hence the EPR signal diminishes and finally vanishes for $T = 200$ K.
- (e) There exists literature showing the EPR signal strength of the oxygen vacancy in dependence on the energy of the incident photons.^[14,79,86,90] We have compiled these data in **Figure 14** and find that the threshold energy to observe V_O^+ is between 1.7 and 2.0 eV. The signal maximum is at about 2.5 eV. In general, the photo cross sections σ_{20} , σ_{21} and σ_{10} (Figure 7) are proportional to the respective transition probabilities^[66] (Figure 6) of the E3 defect center. The photo cross sections σ_{21} and σ_{20} were determined by ODLTS. σ_{10} was only estimated using a simple approximation for photon energies close to the threshold of the $|1\rangle \rightarrow |0\rangle$ transition. In the following we will not use these estimated values and restrict our discussion to energies close to the threshold energy of V_O^+ , even though the increase of σ_{10} qualitatively explains the diminishing of the V_O^+ signal for photon energies above 2.5 eV. The probability for creating the singly occupied state of E3 is $\sigma_{21}/(\sigma_{21} + \sigma_{20})$ (Eq. (16)). The quantitative comparison of $\sigma_{21}/(\sigma_{21} + \sigma_{20})$ and the EPR results is depicted in Figure 14. The current EPR results as well as the dependence of the photo cross section on photon energy resemble the EPR literature data even though, the

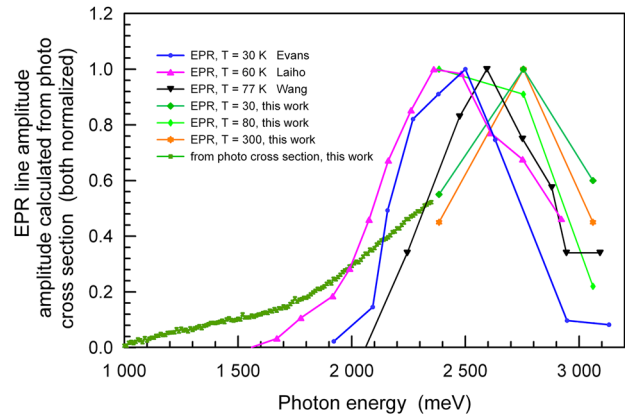


Figure 14. Collection of available literature data^[80,87,14] on the dependence of the V_O^+ EPR signal strength on incident photon energy, our own EPR results and the calculation of the E3 concentration from the photo cross section of the E3 defect as determined by ODLTS (Figure 7).

experimentally determined threshold energy depends on the sensitivity of the experimental setup. For ODLTS the sensitivity of dC/C is better than 10^{-6} . The threshold energy for detection of V_O^+ by EPR is hence not connected to the position of V_O^+ within the band gap of ZnO. The threshold energy for the creation of V_O^+ is at about 1 eV, however, the V_O^+ state has very low concentration since $\sigma_{21} < \sigma_{20}$ for $h\nu \ll 1.7$ eV. Therefore, photon energies above 1.7 eV are required to detect V_O^+ by EPR.

Overall, the currently investigated properties of the E3 deep level defect determined by ODLTS and PL and that of the oxygen vacancy as determined by EPR are strikingly similar.

6. Discussion

Next, a comprehensive model explaining the experimentally derived properties of the deep-level defect E3 is developed and we include: (i) E3 can bind up to two electrons, (ii) E3 is a negative- U center, E3 is involved in a radiative recombination process with maximum intensity at 2.09 eV, and (iii) it resembles properties of the oxygen vacancy.

In order to explain the optical properties of the E3 defect in ZnO, we propose a model (Figure 15) with E3 being a negative- U center. For a negative- U center, the state filled with two electrons is energetically below the single electron state, which means it is stable while the one-electron state is meta-stable (sometimes referred to as an extrinsic Cooper pair^[91]). This is caused by a strong lattice relaxation around the defect when occupied by two electrons, which overcomes the repulsive interaction between the two electrons. For the labeling of the states involved, we introduce $|n, q\rangle$, where n is the electron occupation number of the defect state and q is its configuration coordinate number, i.e., the configuration coordinate normalized by the value of the configuration coordinate of the doubly occupied state. The oxygen vacancy in ZnO may have the states V_O^0 , V_O^+ , and V_O^{2+} . In the case of E3, the states involved are $|2, 2\rangle$, $|1, 1\rangle$, and $|0, 0\rangle$.

If the defect is recharged, both n and q must change. These changes do not in general occur simultaneously, but with a

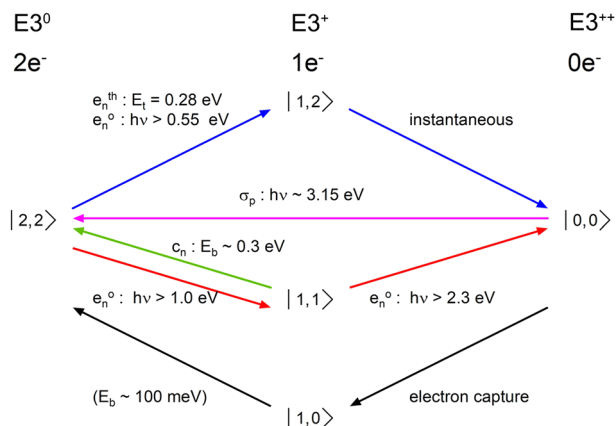


Figure 15. Model for the deep level E3. $|n, q\rangle$ denotes the level filled with n electrons in state q .

certain delay. For the present case of the E3 defect in ZnO, our experiments show that there exists only one transition level changing the occupation of the unoccupied $|0, 0\rangle$ state, and that is the capture of two electrons. The capture of the first electron $|0, 0\rangle \rightarrow |1, 0\rangle$ occurs very quickly, but for the capture of the second electron $|1, 0\rangle \rightarrow |2, 2\rangle$ an energetic barrier of $E_b \approx 100 \text{ meV}^{[63]}$ has to be overcome, while a lattice relaxation and with that a change of q takes place.

This interpretation of the capture process is in concordance with that of Auret et al.^[24] and Chicot et al.^[55] During thermal DLTS measurements, the E3 defect will always emit two electrons due to its negative- U behavior; the thermal activation energy of E3 is about 280 meV. The emission occurs via the meta-stable state $|1, 2\rangle$ having the same configuration coordinate. The electron remaining in the state $|1, 2\rangle$ will be emitted instantaneously into the conduction band and E3 returns via lattice relaxation to the state $|0, 0\rangle$. This implies that the concentration of E3 is only one-half that determined by DLTS or thermally stimulated capacitance measurements, since it always emits two electrons.

If the E3 center is at temperatures too low for a thermal emission (here we used 80 K) illuminated by light with photon energy between 550 meV and 1 eV, both electrons will be optically emitted into the conduction band. This process is similar to the thermal emission $|2, 2\rangle \rightarrow |1, 2\rangle \rightarrow |0, 0\rangle$.

Photon energies above 1 eV are sufficient to optically excite and reconfigure the state $|2, 2\rangle$ to the meta-stable state $|1, 1\rangle$, which cannot be further excited thermally at 80 K. In other words, one electron is excited into the conduction band while the other electron is still bound to E3 and forms the meta-stable one electron state $|1, 1\rangle$. This means that a thermally stimulated transition to $|0, 0\rangle$ is not observed at this temperature. Now, to re-transform the defect from state $|1, 1\rangle$ to the state $|2, 2\rangle$, a thermal energy $E_b \geq 300 \text{ meV}$ is required. Within the optical DLTS measurements the defect E3 is brought to $|2, 2\rangle$ by the filling pulse applied to the sample after each transient measurement.

The ODLTS maximum takes lower and lower values for increasing photon energies (being at least 1 eV) because during one transient measurement more and more transitions to $|1, 1\rangle$ occur until at an energy of 2.40 eV all transitions have $|1, 1\rangle$ as

their final state (Figure 3). Here, the ODLTS maximum takes its minimal value, which corresponds well to about one-half of the ODLTS maximum values measured for photon energies below 1 eV.

The interpretation is in accordance with that of the TSCAP results: E3 undergoes the optically stimulated transition $|2, 2\rangle \rightarrow |1, 1\rangle$. One electron is emitted into the conduction band while the second cannot be thermally or optically emitted (for this temperature and photon energy) and hence the capacitance step is just one-half of that of curve (b) of Figure 5. Within the ODLTS measurements the initial, occupied state of E3 is prepared by the filling pulses prior to each individual measurement. The ODLTS signal for irradiation with photons with an energy of 2350 meV is, at 80 K, roughly one-half of the signal at 150 K, again because only the transition $|2, 2\rangle \rightarrow |1, 1\rangle$ contributes to the signal and at 80 K thermal emission is still negligible. At about 120 K, the thermal emission rate $e_n(T)$ is no longer negligible, and the thermally stimulated transition $|2, 2\rangle \rightarrow |0, 0\rangle$ increasingly contributes to the signal with increasing temperature. Lastly, the thermal emission rate is much larger than the optical rate $e_n(T) \gg e_{20}^0(h\nu)$, so that E3 only emits electrons via $|2, 2\rangle \rightarrow |0, 0\rangle$ thermally. Hence, the DLTS signal increases and has, at about 150 K, twice the height of the 80 K signal. For a photon energy of 2100 meV, not all of the E3 defect levels are transformed to the state $|1, 1\rangle$, and hence some of the E3 defects emitted two electrons thermally ($|2, 2\rangle \rightarrow |0, 0\rangle$). Figure 4c and d reflect the same process but measured with DLTS instead of TSCAP. Irradiation with photon energies higher than 2350 meV enables the transition via $|1, 1\rangle \rightarrow |0, 0\rangle$ and in this regime the number of single electron states $|1, 1\rangle$ decreases with increasing energy of the incident photons. This is indicated in Figure 7 by the strong decrease of $\sigma_{20}^0(h\nu)$. For photon energies higher than 3150 meV, electrons from the valence band can be excited to the two-electron state $|0, 0\rangle \rightarrow |2, 2\rangle$ (σ_p^0). For even higher photon energies, band to band transitions occur (probably involving shallow states) and the photo-ionization cross-section is no longer representative for the E3 defect.

We now turn to the photoluminescence results. E3 is connected to a radiative recombination EB_{E3} having a maximum intensity at 2.09 eV. How can this be incorporated into the model of E3? First of all, the PL measurements were not acquired in a space charge region. In contrast to the ODLTS measurements, free electrons are available during the PL measurement, so that E3 is occupied by electrons for $T < 120 \text{ K}$. At RT, the E3 defect is due to the thermal excitation of electrons into the conduction band not occupied by electrons. In order to attribute EB_{E3} to a transition from a certain state of E3 to another, we make use of the energy balance and develop a Carnot cycle (Figure 16) for the possible charging processes of E3. The state $|2, 2\rangle$ is obtained by starting from state $|0, 0\rangle$ by an optical transition of a valence band electron to E3 with an additional conduction band electron (negative- U center). The state $|1, 1\rangle$ is obtained by irradiation with photon energies above 1 eV. This state is meta-stable and remains unless photons with energy above 2.3 eV are incident on the sample. After the emission of this electron from E3 into the conduction band, the initial state is reached again. The total energy in this process is 3.05 eV and is lower by about 0.3 eV than the band gap. The difference is given to the lattice as phonons. EB_{E3} is now either the transition $|1, 1\rangle \rightarrow |0, 0\rangle$ or $|2, 2\rangle \rightarrow |1, 1\rangle$.

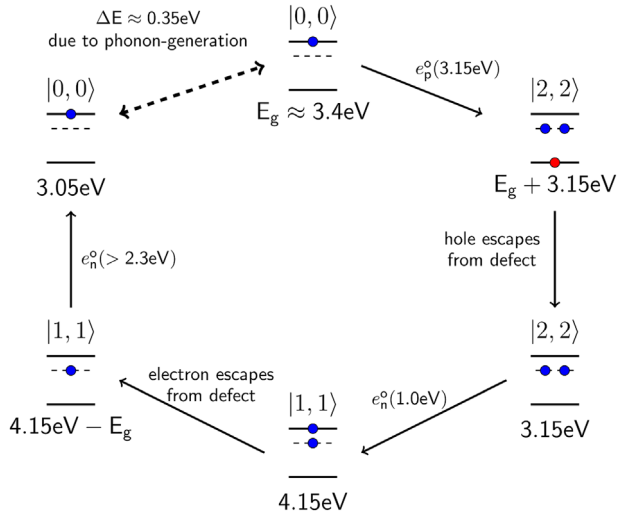


Figure 16. Hypothetical Carnot-cycle of the E3 level with total energy of the system indicated. Initially (topmost panel) the defect is empty and a conduction-band electron is in its vicinity. This electron together with a 3.15 eV photon are captured by the defect and a hole is emitted into the valence-band making E3 become occupied by two electrons. Subsequently one of the electrons bound to E3 can be photo-emitted by a 1.0 eV photon. Finally the remaining electron is photo-emitted by a 2.3 eV photon such that the initial state is restored. During the cycle an energy of about 350 meV is lost which reflects the emitted phonons.

The energy of the state $|1, 1\rangle$ is, according to Figure 16, 4.15 eV. If we subtract the EB_{E3} transition energy, we find that about 2 eV must be transferred to the lattice. For the second possible transition, the initial state is $|2, 2\rangle$ and has an energy of 6.55 eV. Now we subtract again the EB_{E3} transition energy and obtain a value of 4.46 eV, which is higher by about 0.3 eV than the energy of state $|1, 1\rangle$ (4.15 eV). Hence, for $|2, 2\rangle \rightarrow |1, 1\rangle$, only 0.3 eV is transferred to the lattice. We therefore attribute this process to the radiative recombination. This is also in good agreement with the observed spectral broadening and Huang–Rhys factor.

Several first-principles investigations of native point defects in ZnO have been published (Refs. [11,93–105]), and so far the common result of these calculations is that the only intrinsic defect with the negative- U property is the oxygen vacancy. Defect complexes in ZnO with negative- U property have not been predicted until now. However, this does not imply that such defects do not exist. Hence, we have to restrict the following discussion to the only predicted defect with negative- U property.

In n-type ZnO, the Fermi level is typically located close to but below the conduction band minimum (CBM) and the E3 defect level would be occupied by two electrons (at 4 K). The state V_O^+ is meta-stable independently of the position of the Fermi level. The calculated transition energy of the $0 \rightarrow 2+$ transition is between 0.6 eV^[11] and 3 eV^[96] (Table 1) and hence it is argued that the oxygen vacancy is not the source of the native n-type conductivity of ZnO. Boonchun et al.^[104] recently used a new local density approximation and Hubbard U correction approach,^[102] which results in a transition energy of 0.62 eV for the $0 \rightarrow 2+$ transition. Boonchun et al. interpret their results as a verification of the suggestion of Hoffmann et al.^[105] stating that the E4 defect

Table 1. Transition level $\varepsilon(2+/0)$ (equivalent to $|2, 2\rangle \Rightarrow |0, 0\rangle$) measured from the CBM in eV and effective correlation energy U_{cor} in comparison with calculations in the literature.

	$E_c - \varepsilon(2+/0)$	U_{cor}
Thermal experiment	0.28	
Optical experiment	0.55	≈ -1
Zhang et al. ^[11]	0.6	-0.6
Van de Walle ^[92]	0.7	
Janotti et al. ^[93]	1.01	-1
Lany et al. ^[94]	1.8	-1.32
Erhart et al. ^[95]	0.61	
Patterson ^[96]	3	
Lany et al. ^[97]	2.2	
Paudel et al. ^[98]	2.6	-0.05
Oba et al. ^[99]	1.2	
Clark et al. ^[100]	1.21	
Lany et al. ^[101]	1.68	-0.5
Boonchun et al. ^[102]	0.62	-1
Oba et al. ^[104]	1.2	
Boonchun et al. ^[105]	0.62	-1

in ZnO having a thermal activation energy of 580 meV corresponds to the oxygen vacancy. In our bulk single crystals, we could not verify the existence of the E4 defect. The thermal activation energy of E3 is, with about 280 meV, clearly lower than the calculated transition energy of the oxygen vacancy and with respect to that a connection between the two defects seems implausible.

The effective correlation energy U_{cor} , which is the energy necessary to separate the two electrons, has different values in the published calculated results on the oxygen vacancy. Paudel et al.^[98] find $U_{cor} = -0.05$ eV. Janotti et al.^[93] and Boonchun et al.^[102] find $U_{cor} \sim -1$ eV. The latter value corresponds well to the threshold energy of $\sigma_{21}^o(h\nu)$ derived from our ODLTS measurements.

Experimental evidence for E3 being the oxygen vacancy is expected from irradiation/implantation experiments. But again, the published data and their interpretation is not coherent^[16,19–58] and different trends for the change of E3 concentration (including no change at all) were determined after irradiation/implantation or annealing experiments. A connection between E3 and V_O is not suggested by these experiments. In principle, all defects generated within the band gap have to be considered for an unambiguous interpretation of the change of the E3 DLTS signal. In general, the implantation dose should be such that the density of generated defects is lower than two-tenth of the net doping density (exceptions hold true for the C^{2-} DLTS^[106]). In our bulk crystals, the concentration of E3 in the as-received samples is already two-tenth of the net doping density, leaving no room for additional investigations by implantation/irradiation experiments. This means that a combination of implantation/irradiation or annealing experiments and thermal DLTS measurements is in general not sufficient to draw conclusions about the nature of E3, since most of the gap (from the VBM to about 2.6 eV above the VBM) remains unexplored.

7. Summary

We have demonstrated experimentally that the defect level E3 in ZnO can bind two electrons and exhibits the negative- U property. The thermal activation energy of the defect is about 280 meV and corresponds to the emission of two electrons into the conduction band. This transition is attributed to $|2, 2\rangle \rightarrow |0, 0\rangle$. The effective correlation energy of the defect was determined from the measured photo-ionization cross-section σ_{21}^0 to be $U_{\text{cor}} \sim -1$ eV. Further, we revealed that the single electron state $|1, 1\rangle$ can be optically generated for $h\nu > 1$ eV and that this state is stable for temperatures below 100 K. The thermal activation energy for the emission of this process is about 300 meV. In addition, we find that the E3 defect has a radiative recombination for the transition $|2, 2\rangle \Rightarrow |1, 1\rangle$ with a peak maximum energy of 2.09 eV. EPR experiments revealed that the E3 defect resembles properties of the oxygen vacancy such as threshold energy for creation of V_{O}^+ , the dependence of the V_{O}^+ and $E3^+$ signal height on photon energy, and the temperature dependence of the signal height. Comparing the experimental results with first-principles investigations substantiates these similarities. However, the difference between the calculated and experimentally derived thermal activation energies do not allow an unambiguous identification of E3 due to V_{O} . Nevertheless, the results should stimulate further discussions on negative- U centers in ZnO.

Appendix

The exponentially decaying solutions e^{-rt} of the differential Eq. (7) must fulfill $1 = q_0 + q_1 + q_2$ at any time, so that the characteristic polynomial

$$0 = r^2 - (e_{10} + e_{21} + e_{20})r + e_{10}(e_{21} + e_{20}) \quad (8)$$

with zeros at $r_1 = e_{10}$ and $r_2 = e_{21} + e_{20}$ is obtained. At $t=0$, immediately after the DLTS filling pulse, all E3 defects are occupied by two electrons, hence $q_1(t=0) = 0$ and $q_2(t=0) = 1$. This yields

$$\begin{pmatrix} q_1(t) \\ q_2(t) \end{pmatrix} = \begin{pmatrix} \alpha \\ \beta \end{pmatrix} e^{-(e_{21}+e_{20})t} + \begin{pmatrix} \gamma \\ \delta \end{pmatrix} e^{-e_{10}t} \quad (9)$$

In order to determine the constants we shall assume that the emission of the first electron $|2\rangle \rightarrow |1\rangle$ is independent of the emission rate e_{10} for the second electron, which yields $\delta = 0$, $\alpha = -\gamma$, and $\beta = 1$. Furthermore, $\frac{dq_0}{dt}(t=0) = e_{20}q_2(t=0)$ holds since $q_1(t=0) = 0$. Using $\alpha = -\gamma$ we therefore obtain

$$e_{20} = -\frac{dq_2}{dt}(t=0) - \frac{dq_1}{dt}(t=0) \quad (10)$$

$$e_{20} = (e_{21} + e_{20}) + \alpha(e_{21} + e_{20} - e_{10}) \quad (11)$$

$$\alpha = -\frac{e_{21}}{e_{21} + e_{20} - e_{10}}. \quad (12)$$

and the solution of Eq. (7) is

$$\mathbf{q}(t) = \begin{pmatrix} -\frac{e_{21}}{e_{21} + e_{20} - e_{10}} \\ 1 \end{pmatrix} e^{-(e_{21}+e_{20})t} + \begin{pmatrix} \frac{e_{21}}{e_{21} + e_{20} - e_{10}} \\ 0 \end{pmatrix} e^{-e_{10}t}. \quad (13)$$

The time-evolution of the charge state $Q(t)$ (in units of the elementary charge e) of the defect is given by

$$Q(t) = 2 \times q_0(t) + 1 \times q_1(t) + 0 \times q_2(t) \quad (14)$$

(the defect is neutral when occupied by two electrons). With $Q(t=0) = 0$, $Q(t \rightarrow \infty) = 2$ and $q_0 = 1 - q_1 - q_2$, we obtain the general solution

$$Q(t) = 2 + \frac{e_{21}}{e_{21} + e_{20} - e_{10}} e^{-(e_{21}+e_{20})t} - \frac{e_{21}}{e_{21} + e_{20} - e_{10}} e^{-e_{10}t} - 2e^{-(e_{21}+e_{20})t}. \quad (15)$$

In the following, we will discuss this solution for the practically relevant cases (I) $1 \text{ eV} < h\nu < 2.35 \text{ eV}$ and (II) $h\nu > 2.35 \text{ eV}$.

(I) In the first case, $e_{10} = 0$ was experimentally found. Thus Eq. (15) simplifies to

$$Q(t) = 2 + \frac{e_{21}}{e_{21} + e_{20}} e^{-(e_{21}+e_{20})t} - \frac{e_{21}}{e_{21} + e_{20}} - 2e^{-(e_{21}+e_{20})t}, \quad (16)$$

and its limit as $t \rightarrow \infty$ is $Q(t \rightarrow \infty) = 2 - \frac{e_{21}}{e_{21}+e_{20}}$. This yields the limits

$$\begin{aligned} Q(t \rightarrow \infty, e_{21} = 0) &= 2 \quad \text{and} \\ Q(t \rightarrow \infty, e_{21} \rightarrow \infty) &= 1. \end{aligned} \quad (17)$$

In other words, depending on the emission rate e_{21} , the charge state of the defect after a long time will be in between 1 and 2.

We now discuss the consequences of these results for a DLTS experiment. For simplicity, a simple lock-in correlation function will be used for the calculation of the DLTS signal:

$$S(\tau) = \frac{1}{2\tau} \left(\int_0^\tau Q(t) dt - \int_\tau^{2\tau} Q(t) dt \right) \quad (18)$$

with

$$\int Q(t) dt = at - a \frac{1}{e_{21} + e_{20}} e^{-(e_{21}+e_{20})t} \quad (19)$$

with

$$a = 2 - \frac{1}{1 + \frac{e_{20}}{e_{21}}}. \quad (20)$$

This yields

$$S(\tau) = -a \times \underbrace{\frac{2}{(e_{21} + e_{20})\tau} \left(1 - e^{-(e_{21}+e_{20})\tau} \right)^2}_{\text{DLTS signal with } e=e_{21}+e_{20}} \quad (21)$$

In **Figure 17**, this solution is displayed for different values of e_{20} and e_{21} . The maximum S of $S(T)$ is a function of $\frac{e_{20}}{e_{21}}$. The absolute maximum of the DLTS signal S_{\max} is reached for $e_{21} = 0$. In the following, S_{\max} will be normalized at two electron charges, so that $S_{\max} = 2$ holds. For $e_{21} > 0$, we obtain $1 < S(\frac{e_{20}}{e_{21}}) < 2 = S_{\max}$. If S_{\max} can be experimentally determined, in the case of E3 this was possible for $T = 80$ K and $h\nu \approx 0.8$ eV, then e_{21} and e_{20} can be calculated for any other DLTS experiment (provided $e_{10} = 0$, as assumed) from

$$\frac{S(\frac{e_{20}}{e_{21}})}{S_{\max}} = \frac{2e_{20} + e_{21}}{2(e_{21} + e_{20})} \quad \text{and} \quad e_{\text{rate}} = e_{21} + e_{20} \quad (22)$$

with e_{rate} being the emission rate in the maximum of $S(\frac{e_{20}}{e_{21}})$ or, in other words, e_{rate} fits the chosen emission rate. The two Eq. (16) for the two unknowns can be solved:

$$\begin{aligned} e_{21} &= 2e_{\text{rate}} \left(1 - \frac{S(\frac{e_{20}}{e_{21}})}{S_{\max}} \right) \quad \text{and} \\ e_{20} &= e_{\text{rate}} \left(2 \frac{S(\frac{e_{20}}{e_{21}})}{S_{\max}} - 1 \right). \end{aligned} \quad (23)$$

(II) In the second case, $h\nu > 2.35$ eV, then an optical emission from E3 defects occupied by only one electron $|1\rangle \rightarrow |0\rangle$ is also possible, hence $e_{10} > 0$ holds. Therefore, no approximation of Eq. (15) is possible and the charge state of the defect is

$$Q(t) = 2 - \left(2 - \frac{1}{1 + \frac{e_{20} - e_{10}}{e_{21}}} \right) e^{-(e_{21} + e_{20})t} - \frac{1}{1 + \frac{e_{20} - e_{10}}{e_{21}}} e^{-e_{10}t}. \quad (24)$$

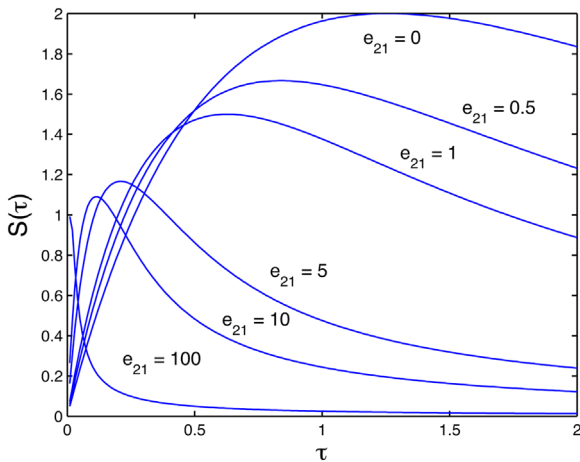


Figure 17. DLTS signal $S(\tau)$ for $e_{20} = 1$ and $e_{21} = (0, 0.5, 1, 5, 10, 100)$.

The constraints and pre-conditions considered earlier are fulfilled and the DLTS signal can be calculated using Eq. (18):

$$S(\tau) = - \underbrace{\left(2 - \frac{1}{1 + \frac{e_{20} - e_{10}}{e_{21}}} \right)}_{\text{pre-factor}} \times \underbrace{\frac{2}{(e_{21} + e_{20})\tau} (1 - e^{-(e_{21} + e_{20})\tau})^2}_{\text{DLTS-signal1}} - \underbrace{\frac{1}{1 + \frac{e_{20} - e_{10}}{e_{21}}}}_{\text{pre-factor}} \times \underbrace{\frac{2}{e_{10}\tau} (1 - e^{-e_{10}\tau})^2}_{\text{DLTS-signal2}}. \quad (25)$$

In the experiment, the emission from the defect appears as a superposition of two DLTS signals.

Acknowledgements

The authors acknowledge Martin W. Allen for fruitful discussions and the fabrication of the Schottky barrier diodes. Further, we thank Florian Schmidt for helpful discussions and proofreading. Parts of this work have been supported by Deutsche Forschungsgemeinschaft in the framework of SFB 762. We acknowledge support by Universität Leipzig within research profile area “Complex Matter”.

Conflict of Interest

The authors declare no conflict of interest.

Keywords

deep level defects, DLTS, EPR, negative- U center, ODLTS, oxygen vacancy, photoluminescence, ZnO

Received: December 12, 2017

Revised: January 26, 2018

Published online:

- [1] Ü. Özgür, Y. I. Alivov, C. Liu, A. Teke, M. A. Reshchikov, S. Dogan, V. Avrutin, S.-J. Cho, H. Morkov, *J. Appl. Phys.* **2005**, 98, 041301.
- [2] H. Frenzel, M. Lorenz, F. Schein, A. Lajn, *Phys. Status Solidi B* **2004**, 241, 231.
- [3] H. von Wenckstern, R. Schmidt-Grund, C. Bundesmann, A. Müller, C. P. Dietrich, M. Stölzel, M. Lange, M. Grundmann, *Handbook of Zinc Oxide and Related Materials*, Taylor & Francis, FL, USA **2012**.
- [4] S. Lany, J. Osorio-Guillén, A. Zunger, *Phys. Rev. B* **2007**, 75, 241203.
- [5] M. D. McCluskey, S. J. Jokela, *J. Appl. Phys.* **2009**, 106, 071101.
- [6] V. Avrutin, D. J. Silversmith, H. Morkoc, *Proc. IEEE* **2010**, 98, 1269.
- [7] B. K. Meyer, H. Alves, D. M. Hofmann, W. Kriegeis, D. Forster, F. Bertram, J. Christen, A. Hoffmann, M. Straßburg, M. Dworzak, U. Haboeck, A. V. Rodina, *Phys. Status Solidi B* **2004**, 241, 231.
- [8] J. Robertson, R. Gillen, S. J. Clark, *Thin Solid Films* **2012**, 520, 3714.
- [9] Y. Yan, S. Wei, *Phys. Status Solidi B* **2008**, 245, 641.
- [10] C. H. Park, S. B. Zhang, S. Wei, *Phys. Rev. B* **2002**, 66, 073202.

- [11] S. B. Zhang, S. Wei, A. Zunger, *Phys. Rev. B* **2001**, 63, 075205.
- [12] L. S. Vlasenko, G. D. Watkins, *Phys. Rev. B* **2005**, 71, 125210.
- [13] L. S. Vlasenko, G. D. Watkins, *Phys. Rev. B* **2005**, 72, 035203.
- [14] X. J. Wang, L. S. Vlasenko, S. J. Pearton, W. M. Chen, I. A. Buyanova, *J. Phys. D: Appl. Phys.* **2009**, 42, 175411.
- [15] F. A. Selim, M. H. Weber, D. Solodovnikov, K. G. Lynn, *Phys. Rev. Lett.* **2007**, 99, 085502.
- [16] F. Schmidt, H. von Wenckstern, O. Breitenstein, R. Pickenhain, M. Grundmann, *Solid-State Electron.* **2014**, 92, 40.
- [17] S. Brehme, R. Pickenhain, *Phys. Status Solidi A* **1985**, 88, K63.
- [18] A. Chantre, G. Vincent, D. Bois, *Phys. Rev. B* **1981**, 23, 5335.
- [19] M. Ellguth, M. Schmidt, R. Pickenhain, H. von Wenckstern, M. Grundmann, *Phys. Status Solidi B* **2011**, 248, 941.
- [20] A. Nitayama, H. Sakaki, T. Ikoma, *Jpn. J. Appl. Phys.* **1980**, 19, L743.
- [21] A. Rohatgi, S. K. Pang, T. K. Gupta, W. D. Straub, *J. Appl. Phys.* **1988**, 63, 5375.
- [22] J. C. Simpson, J. F. Cordaro, *J. Appl. Phys.* **1988**, 63, 1781.
- [23] F. D. Aurret, S. A. Godman, M. Hayes, M. J. Legodi, H. A. van Laarhoven, D. C. Look, *Appl. Phys. Lett.* **2001**, 79, 3074.
- [24] F. D. Aurret, S. A. Goodman, M. J. Legodi, W. E. Meyer, D. C. Look, *Appl. Phys. Lett.* **2002**, 80, 1340.
- [25] A. Y. Polyakov, N. B. Smirnov, A. V. Govorkov, E. A. Kozhukhova, V. I. Vdovin, K. Ip, M. E. Overberg, Y. W. Heo, D. P. Norton, S. J. Pearton, J. M. Zavada, V. A. Dravin, *J. Appl. Phys.* **2003**, 94, 2895.
- [26] G. Brauer, W. Anwand, W. Skorupa, J. Kuriplach, O. Melikhova, H. von Wenckstern, H. Schmidt, M. Lorenz, M. Grundmann, *Phys. Rev. B* **2006**, 74, 045208.
- [27] Y. Jiang, N. C. Giles, L. E. Halliburton, *J. Appl. Phys.* **2007**, 101, 093706.
- [28] H. von Wenckstern, M. Brandt, H. Schmidt, G. Biehne, R. Pickenhain, H. Hochmuth, M. Lorenz, M. Grundmann, *Appl. Phys. A* **2007**, 88, 135.
- [29] T. Frank, G. Pensl, R. Tena-Zaera, J. Zuniga-Perez, C. Martinez-Thomas, V. Munoz-Sanjose, T. Ohshima, H. Itoh, D. Hoffmann, D. Pfisterer, J. Sann, B. Meyer, *Appl. Phys. A* **2007**, 88, 141.
- [30] H. von Wenckstern, H. Schmidt, M. Grundmann, M. W. Allen, P. Miller, R. J. Reeves, S. M. Durbin, *Appl. Phys. Lett.* **2007**, 91, 022913.
- [31] M. Hayes, F. D. Aurret, P. J. Janse van Rensburg, J. M. Nel, W. Wesch, E. Wendler, *Phys. Status Solidi B* **2007**, 244, 1544.
- [32] H. Frenzel, H. von Wenckstern, A. Weber, H. Schmidt, G. Biehne, H. Hochmuth, M. Lorenz, M. Grundmann, *Phys. Rev. B* **2007**, 76, 035214.
- [33] F. D. Aurret, W. Meyer, P. J. van Rensburg, M. Hayes, J. Nel, H. von Wenckstern, H. Schmidt, G. Biehne, H. Hochmuth, M. Lorenz, M. Grundmann, *Physica B* **2007**, 401-402, 278.
- [34] Z. Q. Fang, B. Claflin, D. C. Look, Y. F. Dong, H. L. Mosbacker, L. J. Brillson, *J. Appl. Phys.* **2008**, 104, 063707.
- [35] Q. L. Gu, C. C. Ling, G. Brauer, W. Anwand, W. Skorupa, Y. F. Hsu, A. B. Djurrisic, C. Y. Zhu, S. Fung, L. W. Lu, *Appl. Phys. Lett.* **2008**, 92, 222109.
- [36] H. von Wenckstern, G. Biehne, M. Lorenz, M. Grundmann, F. D. Aurret, W. E. Meyer, P. J. J. van Rensburg, M. Hayes, J. N. Nel, *J. Korean Phys. Soc.* **2008**, 53, 2861.
- [37] Z. Q. Fang, B. Claflin, D. C. Look, Y. F. Dong, L. Brillson, *J. Vac. Sci. Technol. B* **2009**, 27, 1774.
- [38] M. Schmidt, M. Ellguth, C. Czekalla, H. von Wenckstern, M. Grundmann, G. Brauer, W. Skorupa, M. Helm, Q. Gu, C. C. Ling, *J. Vac. Sci. Technol. B* **2009**, 27, 1597.
- [39] L. Vines, E. V. Monakhov, B. G. Svensson, *Physica B: Phys. Condens. Matter* **2009**, 404, 4386.
- [40] Y. Dong, Z. Q. Fang, D. C. Look, D. R. Doust, G. Cantwell, J. Zhang, J. J. Song, L. J. Brillson, *J. Appl. Phys.* **2010**, 108, 103718.
- [41] L. Vines, E. V. Monakhov, R. Schifano, W. Mtangi, F. D. Aurret, B. G. Svensson, *J. Appl. Phys.* **2010**, 107, 103707.
- [42] H. von Wenckstern, K. Brachwitz, M. Schmidt, C. P. Dietrich, M. Ellguth, M. Stölzel, M. Lorenz, M. Grundmann, *J. Electron. Mater.* **2010**, 39, 584.
- [43] V. Quemener, L. Vines, E. V. Monakhov, B. G. Svensson, *Int. J. Appl. Ceram. Technol.* **2010**, 8, 1017.
- [44] V. Quemener, L. Vines, E. V. Monykov, B. G. Svensson, *Appl. Phys. Lett.* **2011**, 99, 112112.
- [45] L. Vines, J. Wong-Leung, C. Jagadish, E. V. Monakhov, B. G. Svensson, *Physica B: Phys. Condens. Matter* **2011**, 1.
- [46] M. Schmidt, K. Brachwitz, F. Schmidt, M. Ellguth, H. von Wenckstern, R. Pickenhain, M. Grundmann, G. Brauer, W. Skorupa, *Phys. Status Solidi B* **2011**, 248, 1949.
- [47] L. Scheffler, V. I. Kolkovsky, E. V. Lavrov, J. Weber, *J. Phys. Condens. Matter* **2011**, 23, 334208.
- [48] F. Schmidt, H. von Wenckstern, D. Spemann, M. Grundmann, *Appl. Phys. Lett.* **2012**, 101, 012103.
- [49] L. Vines, J. Wong-Leung, C. Jagadish, V. Quemener, E. V. Monakhov, B. G. Svensson, *Appl. Phys. Lett.* **2012**, 100, 212106.
- [50] V. Quemener, L. Vines, E. V. Monakhov, B. G. Svensson, *Appl. Phys. Lett.* **2012**, 100, 112108.
- [51] W. Mtangi, A. D. Aurret, W. E. Meyer, M. J. Legodi, P. J. Janse van Rensburg, S. M. M. Coelho, M. Diale, J. M. Nel, *J. Appl. Phys.* **2012**, 111, 094504.
- [52] W. Mtangi, A. D. Aurret, M. Diale, W. E. Meyer, A. Chawanda, H. de Meyer, P. J. Janse van Rensburg, J. M. Nel, *J. Appl. Phys.* **2012**, 111, 084503.
- [53] M. Schmidt, H. von Wenckstern, R. Pickenhain, M. Grundmann, *Solid-State Electron.* **2012**, 75, 48.
- [54] W. Mtangi, M. Schmidt, F. D. Aurret, W. E. Meyer, P. J. Janse van Rensburg, M. Diale, J. M. Nel, A. G. Das, F. C. C. Lung, A. Chawanda, *J. Appl. Phys.* **2013**, 113, 124502.
- [55] G. Chicot, J. Pernot, J. Santailier, C. Granier, P. Ferret, A. Ribeaudo, G. Feuillet, P. Muret, *Phys. Status Solidi B* **2013**, 251, 206.
- [56] F. Schmidt, S. Müller, H. von Wenckstern, G. Benndorf, R. Pickenhain, M. Grundmann, *J. Appl. Phys.* **2014**, 116, 103703.
- [57] A. Hupfer, C. Bhodoo, L. Vines, B. G. Svensson, *Appl. Phys. Lett.* **2014**, 104, 092111.
- [58] G. Chicot, P. Muret, J. L. Santailier, G. Feuillet, *J. Phys. D: Appl. Phys.* **2014**, 47, 465103.
- [59] S. Lautenschlaeger, S. Eisermann, M. N. Hofmann, U. Roemer, M. Pinnisch, A. Laufer, B. K. Meyer, H. von Wenckstern, A. Lajn, F. Schmidt, M. Grundmann, J. Blaessing, A. Krost, *J. Cryst. Growth* **2010**, 312, 2078.
- [60] J. Chai, R. J. Mendelsberg, R. J. Reeves, J. Kennedy, H. von Wenckstern, M. Schmidt, M. Grundmann, K. Doyle, T. H. Myers, S. M. Durbin, *J. Electron. Mater.* **2010**, 39, 577.
- [61] M. W. Allen, P. Miller, R. J. Reeves, S. M. Durbin, *Appl. Phys. Lett.* **2007**, 90, 062104.
- [62] D. V. Lang, *J. Appl. Phys.* **1974**, 45, 3023.
- [63] M. Schmidt, Dissertation Universität Leipzig, **2012**.
- [64] G. Goto, Y. Adachi, T. Ikoma, *Jpn. J. Appl. Phys.* **1979**, 18, 1979.
- [65] J. Bourgoin, M. Lannoo, *Point Defects in Semiconductors II*, Springer-Verlag, Berlin **1983**.
- [66] M. Jaros, *Phys. Rev. B* **1977**, 16, 3694.
- [67] G. Lucovsky, *Solid State Commun.* **1965**, 3, 299.
- [68] P. Blood, J. W. Orton, *The Electrical Characterisation of Semiconductors: Majority Carriers and Electron States*, Academic Press Limited, London **1992**.
- [69] A. Janotti, C. G. van de Walle, *Rep. Prog. Phys.* **2009**, 72, 126501.
- [70] P. W. Anderson, *Phys. Rev. Lett.* **1975**, 34, 953.
- [71] P. A. Rodnyi, I. V. Khodyuk, *Opt. Spectrosc.* **2011**, 111, 776.
- [72] M. A. Reshchikov, H. Morkoç, B. Nemeth, J. Nause, J. Xie, B. Hertog, A. Osinsky, *Physica B* **2007**, 401-402, 358.

- [73] F. H. Leiter, H. R. Alves, A. Hofstaetter, D. M. Hofmann, B. K. Meyer, *Phys. Status Solidi B* **2001**, 226, R4.
- [74] S. Seto, S. Yamada, K. Suzuki, K. Yoshino, *J. Korean Phys. Soc.* **2008**, 53, 2959.
- [75] C. H. Ahn, Y. Y. Kim, D. C. Kim, S. K. Mohanta, H. K. Cho, *J. Appl. Phys.* **2009**, 105, 013502.
- [76] P. B. Dorain, *Phys. Rev.* **1958**, 112, 1058.
- [77] A. Hausmann, *Phys. Status Solidi* **1969**, 31, K131.
- [78] W. W. Walsh, L. W. Rupp, *Phys. Rev.* **1962**, 126, 952.
- [79] S. M. Evans, N. C. Giles, L. E. Halliburton, L. A. Kappers, *J. Appl. Phys.* **2008**, 103, 043710.
- [80] O. F. Schirmer, *J. Phys. Chem. Solids* **1968**, 29, 1407.
- [81] C. Gonzales, D. Block, R. T. Cox, A. Herve, *J. Cryst. Growth*, **1982**, 59, 357.
- [82] H. von Wenckstern, G. Biehne, R. A. Rahman, H. Hochmuth, M. Lorenz, M. Grundmann, *Appl. Phys. Lett.* **2006**, 88, 092102.
- [83] J. M. Smith, W. E. Vehse, *Phys. Lett.* **1970**, 147, 31A.
- [84] C. Gonzales, D. Galland, A. Herve, *Phys. Status Solidi A* **1975**, 72, 309.
- [85] A. Hausmann, B. Schallenger, *Z. Physik B* **1978**, 31, 269.
- [86] R. Laiho, L. S. Vlasenko, M. P. Vlasenko, *J. Appl. Phys.* **2008**, 10, 123709.
- [87] A. Pöppl, G. Völkel, *Phys. Status Solidi A* **1991**, 125, 572.
- [88] R. Laiho, D. S. Poloskin, Yu. P. Stepanov, M. P. Vlasenko, L. S. Vlasenko, V. S. Zakahvalinskii, *J. Appl. Phys.* **2009**, 106, 013712.
- [89] Y. Twig, E. Suhovoy, A. Blank, *Rev. Sci. Instrum.* **2010**, 81, 104703.
- [90] L. S. Vlasenko, *Physica B* **2009**, 404, 4774.
- [91] G. D. Watkins, *Advances in Solid State Physics*, Springer-Verlag, Berlin **1984**, p. 163.
- [92] C. G. Van de Walle, *Physica B* **2001**, 308–310, 899.
- [93] A. Janotti, C. Van de Walle, *Appl. Phys. Lett.* **2005**, 87, 122102.
- [94] S. Lany, A. Zunger, *Phys. Rev. B* **2005**, 72, 035215.
- [95] P. Erhart, K. Albe, A. Klein, *Phys. Rev. B* **2006**, 73, 205203.
- [96] C. H. Patterson, *Phys. Rev. B* **2006**, 74, 14432.
- [97] S. Lany, A. Zunger, *Phys. Rev. Lett.* **2007**, 98, 045501.
- [98] T. R. Paudel, W. R. L. Lambrecht, *Phys. Rev. B* **2008**, 77, 205202.
- [99] F. Oba, A. Togo, I. Tanaka, J. Paier, G. Kresse, *Phys. Rev. B* **2008**, 77, 245202.
- [100] S. J. Clark, J. Robertson, S. Lany, A. Zunger, *Phys. Rev. B* **2010**, 81, 115311.
- [101] S. Lany, A. Zunger, *Phys. Rev. B* **2010**, 81, 113201.
- [102] A. Boonchun, W. R. L. Lambrecht, *Phys. Status Solidi B* **2011**, 248, 1043.
- [103] F. Oba, M. Choi, A. Togo, I. Tanaka, *Sci. Technol. Adv. Mater.* **2011**, 12, 034302.
- [104] A. Boonchun, W. R. L. Lamprecht, *Phys. Status Solidi B* **2013**, 250, 2091.
- [105] D. M. Hoffmann, D. Pfisterer, J. Sann, B. K. Meyer, R. Tena-Zaera, V. Munoz-Sanjose, G. Pensl, *Appl. Phys. A* **2007**, 88, 147.
- [106] H. Okushi, Y. Tokumaru, *Jpn. J. Appl. Phys.* **1981**, 20, L45.